

Reorientational and translational dynamics of benzene in zeolite NaY as studied by one- and two-dimensional exchange spectroscopy and static-field-gradient nuclear magnetic resonance^{a)}

B. Geil^{b)}

Fachbereich Physik, TU Darmstadt, 64289 Darmstadt, Germany

O. Isfort

Fachbereich Physik, Universität Dortmund, 44221 Dortmund, Germany

B. Boddenberg

Fachbereich Chemie, Universität Dortmund, 44221 Dortmund, Germany

D. E. Favre and B. F. Chmelka

Department of Chemical Engineering, University of California, Santa Barbara, California 93106

F. Fujara

Fachbereich Physik, TU Darmstadt, 64289 Darmstadt, Germany

(Received 16 July 2001; accepted 31 October 2001)

One- and two-dimensional ²H- and ¹³C-NMR (nuclear magnetic resonance) echo spectroscopy and ¹H static field gradient NMR self-diffusion experiments have been used to study the reorientational and translational dynamics of benzene molecules adsorbed on zeolite NaY as a function of loading. Comparison of the data with model calculations establish that the elementary motional process of the guest molecules is consistently identified as a jump process among well defined adsorption sites inside a supercage and/or a jump between nearby supercages. In cases where the zeolite cavities contain high loadings of guest molecules, each molecular jump is accompanied by concomitant relaxation of the local environment. Molecular jump events between adsorption sites correspond to the elementary processes from which long range translational diffusion evolves. © 2002 American Institute of Physics. [DOI: 10.1063/1.1429646]

I. INTRODUCTION

The dynamics of molecular guest species in zeolite cavities determine the properties of these materials when applied as catalysts, ion exchangers or molecular sieves.^{1–3} The mechanisms of molecular mobility largely depend on both topological restrictions of the pores and interactions with charge balancing cationic adsorption sites associated with the zeolite framework. The present work, being a detailed extension of a preceding letter,⁴ deals with the dynamics of benzene molecules adsorbed on the synthetic Faujasite-type zeolite NaY.

A number of recent studies have employed solid-state NMR spectroscopy to characterize complicated site-hopping motions undergone by strongly adsorbed hydrocarbon molecules on zeolites.^{5–7} We have previously used ²H two-dimensional (2D) exchange NMR experiments⁴ to study slow dynamic processes of perdeuterated benzene molecules in NaY at virtually complete pore loading (5.1 molecules per supercage). Over the temperature range 250–270 K, the benzene molecules were shown to undergo thermally activated ($E_a \cong 40$ kJ/mol) reorientational jumps among the (approximately) tetrahedrally arranged six-ring cation and twelve-ring window adsorption sites, the correlation times being of

the order of a few milliseconds. Each such jump event is accompanied by essentially instantaneous relaxation of the near environment, resulting in small angle reorientations of molecules at neighboring adsorption sites. The benzene dynamics were shown to be characterized by a distribution of motional correlation times, which is attributed to partial disorder of Na⁺ cation siting.

Most importantly, the connection between discrete molecular jump reorientation events and long range translational diffusion properties remains to be established. This is pursued in the present paper by extending the measurements to a wider temperature range, by reducing the concentration of adsorbed benzene molecules, and by applying an enlarged set of NMR techniques that are sensitive to local, as well as mesoscopic, structures, and dynamics.

II. METHODS

A combination of complementary solid-state NMR techniques have been applied to probe and compare directly the nano- and mesoscopic guest transport properties of the benzene–NaY zeolite system. Specifically, the methods used fall under four different categories of pulsed solid-state NMR experiments, namely (1) one-dimensional (1D) echo ²H and ¹³C spectra; (2) 2D exchange ²H and ¹³C spectra; (3) 2D ²H echo decay curves; (4) ¹H diffusion measurements in a static magnetic-field gradient. Before summarizing these experi-

^{a)}This paper is dedicated to Professor Hans Sillescu on his 65th birthday.

^{b)}Author to whom correspondence should be addressed. Electronic mail: burkhard.geil@physik.tu-darmstadt.de

ments, we describe how stochastic processes can be modeled and incorporated into functional forms that are suitable for the analysis of NMR data.

A. Stochastic processes

Following Sillescu,⁸ elementary molecular motional processes taking place in thermal equilibrium can be treated as stationary Markov processes. For instance, the reorientation of a molecule from orientation Ω_1 at a time t_1 to Ω_2 at time t_2 can be described by a conditional probability density (using the notation of van Kampen⁹)

$$P_{1|1}(\Omega_2, t_2 | \Omega_1, t_1) = P_{1|1}(\Omega_2, t | \Omega_1, 0), \quad (1)$$

with $t = t_2 - t_1$. All specific motional models are formulated as discrete N site models (with possible orientations Ω_i , $i = 1 \cdots N$), such that the transition probabilities $P_{ij}(t) = P_{1|1}(\Omega_i, t | \Omega_j, 0)$ are found by solving a master equation

$$\frac{d}{dt} P_{ij}(t) = \sum_{k=1, k \neq i}^N \{W_{ik} P_{kj}(t) - W_{ki} P_{ij}(t)\}, \quad (2)$$

with the transition rate W_{ij} . The terms W_{ij} obey the detailed balance condition, $W_{ij} p_j = W_{ji} p_i$, with a time-independent *a priori* probability p_i for the occupation of site i . If we define the exchange matrix Π by

$$\Pi_{ij} = W_{ij} - \delta_{ij} \sum_{k=1, k \neq i}^N W_{ki}, \quad (3)$$

the master equation [Eq. (2)] simplifies to

$$\frac{d}{dt} P_{ij}(t) = \sum_{k=1}^N \Pi_{ik}(t) P_{kj}(t), \quad (2a)$$

or, in matrix notation, using $\mathbf{P}(t) = \{P_{ij}(t)\}$

$$\frac{d}{dt} \mathbf{P}(t) = \Pi \mathbf{P}(t). \quad (2b)$$

The solution $\mathbf{P}(t)$ is related to the spectroscopic correlation functions measured in 2D NMR, as shown below.

B. Reorientation models

As previously shown the benzene molecules are expected to perform tetrahedral reorientational jumps while hopping from one adsorption site to a neighboring position.^{4,5} The four molecular orientations, as represented by the normal vectors of the benzene rings, can be characterized by a set of Euler angles $\Omega_1 = (0^\circ, 0^\circ, 0^\circ)$, $\Omega_2 = (0^\circ, 109^\circ, 0^\circ)$, $\Omega_3 = (120^\circ, 109^\circ, 0^\circ)$, and $\Omega_4 = (240^\circ, 109^\circ, 0^\circ)$. Jump exchange events that occur among these orientations are described by the rate matrix

$$\Pi = \begin{pmatrix} -3w & w & w & w \\ w & -3w & w & w \\ w & w & -3w & w \\ w & w & w & -3w \end{pmatrix}. \quad (4)$$

From the three nonvanishing degenerate eigenvalues $\Lambda_{1,2,3} = -4w$, we can deduce the correlation time $\tau_c = (4w)^{-1}$.

Because the four tetrahedrally arranged cation sites are related to the tetrahedrally arranged window sites by inversion at the cage center, a given orientation Θ with respect to the magnetic field direction cannot be distinguished from $180^\circ - \Theta$ (see Sec. IID, below). In this sense, “tetrahedral jumps” imply the possibility that molecules will encounter all (cation and window) adsorption sites.

We will also consider “quasi-tetrahedral” jump models, where a large number of additional orientations in the vicinity of the four tetrahedral orientations are assumed.¹⁰ Such models serve to mimic orientational disorder in the benzene subsystem. Details will be discussed in the context of experimental results below.

C. Distribution of correlation times

Besides the above described orientational disorder in the benzene subsystem, structural disorder, e.g., due to a non-equivalence of adsorption sites, is accompanied by a distribution of motional correlation times.¹¹ As will be shown below, the parametrization of the experimental curves indicates that such a distribution is appropriate for the benzene–NaY zeolite system. Here, we assume a logarithmic Gaussian distribution

$$g(\tau_c) \propto \exp\left[-\frac{(\ln \tau_c - \ln \tau_{\max})^2}{2\sigma_\tau^2}\right], \quad (5)$$

with a width parameter σ_τ and a maximum at τ_{\max} . The mean correlation time (first moment), $\langle \tau_c \rangle$, is given by

$$\langle \tau_c \rangle = \int_{-\infty}^{\infty} \tau_c g(\tau_c) d \ln \tau_c = \tau_{\max} \exp\left[\frac{3}{2}\sigma_\tau^2\right]. \quad (6)$$

Because the functional form of $g(\tau_c)$ cannot be explicitly established *a priori* or from experiment, the assumed shape represents a parametrization. On the other hand, the choice of a log-Gaussian distribution is physically motivated: If the temperature dependence of τ_c follows an Arrhenius type law, $\tau_c \sim \exp(E_a/RT)$, then a Gaussian distribution of potential wells will lead to a log-Gaussian distribution of correlation times.

D. Experiments

Solid-state ^1H , ^2H , and ^{13}C NMR experiments were performed to obtain complementary information about the dynamic behavior of adsorbed benzene guest molecules from the different nuclei. ^1H NMR measurements were conducted in the presence of a strong static field gradient, which permits macroscopic benzene diffusivities to be determined. In the case of ^2H NMR, the Larmor frequency, ω_0 , in the high-field limit is given by $\omega_0 = \omega_Z + \omega_Q$, where ω_Z is the Zeeman frequency, and the quadrupolar frequency, $\omega_Q = \pm \delta/2[(3 \cos^2 \Theta - 1) - \eta \sin^2 \Theta \cos(2\Phi)]$. For the temperatures used here, the benzene molecules undergo fast ($\ll 10^{-6}$ s) hexad axis rotational dynamics,^{5,12,13} so that the residual quadrupolar coupling constant $\delta = 2\pi \cdot 69$ kHz, and the asymmetry parameter $\eta = 0$. Under these circumstances, Θ denotes the angle of the molecule normal axis relative to the applied magnetic field direction. In a powder, this leads to the well-known Pake spectrum. In the case of ^{13}C NMR,

the resonance frequency is given by a similar expression, $\omega_0 = \omega_z(1 - \sigma_{\text{iso}}) + \frac{1}{2}\delta[(3 \cos^2 \Theta - 1) - \eta \sin^2 \Theta \cos(2\Phi)]$, except that here, ω_z is modified by the isotropic chemical shift, σ_{iso} , and the spectrum is asymmetric. At an applied field of 4.23 Tesla, which corresponds to a ^{13}C Zeeman frequency of 45.3 MHz, the effective coupling constant for benzene molecules undergoing fast uniaxial rotation is found to be $\delta = 2\pi$ 5.5 kHz and $\eta = 0$. Descriptions of the four specific NMR experiments follow below:

1. One-dimensional (1D) ^2H and ^{13}C echo spectra

Following Greenfield *et al.*,¹⁴ the time dependence of the coupling tensors can be described by the general equation

$$\frac{d}{dt} \boldsymbol{\sigma}(t) = (i\boldsymbol{\omega} + \mathbf{\Pi}) \boldsymbol{\sigma}(t) = \mathbf{A} \boldsymbol{\sigma}(t), \quad (7)$$

where the individual components σ_i of $\boldsymbol{\sigma}$ are attributed to different molecular orientations Ω_i ($i = 1 \cdots N$). The diagonal matrix $\boldsymbol{\omega}$ contains the quadrupolar (or chemical shift) contributions $\omega_i = \delta/2(3 \cos^2 \Theta_i - 1)$, and $\mathbf{\Pi}$ is the exchange matrix defined in Eq. (3). Solving Eq. (7) leads to the desired quantity, the powder averaged deuteron magnetization after the second pulse of the experimental 1D sequence (pulse)- τ (pulse)

$$M(t) = \langle \mathbf{1}^T \exp[\mathbf{A}(t - \tau)] \exp[\mathbf{A}^*(\tau)] \boldsymbol{\sigma}(0) \rangle_{\text{powder}}. \quad (8)$$

The powder average is calculated numerically following the algorithm of Alderman *et al.*¹⁵ 1D echo measurements yield information about molecular jump rates that occur at frequencies within the order of the effective coupling constant δ and that are greater than the transverse relaxation rate T_2^{-1} .

2. Two-dimensional ^2H and ^{13}C (2D) exchange spectra

Our treatment of 2D NMR spectroscopy is largely based upon that of Schmidt-Rohr and Spiess.¹⁶ The echo amplitude of an idealized “stimulated echo” three-pulse sequence, (pulse)- t_1 -(pulse)- t -(pulse)- t_2 , is given by the following correlation function:

$$F(t_1, t_2, t) = \langle e^{-i\omega_1 t_1} e^{+i\omega_2 t_2} \rangle. \quad (9)$$

In this formulation, ω_1 is identified with the local frequency at time $t = 0$ and ω_2 with that at a later time t . For a given N site model, this correlation function can be reformulated in terms of transition probabilities $P_{ij}(t)$. For example, in the case of ^2H NMR, one obtains

$$F(t_1, t_2, t) = \sum_{i,j=1}^N \langle \exp[-i\omega_Q(\theta_i)t_1] \times \exp[i\omega_Q(\theta_j)t_2] \rangle_{\text{powder}} p_i P_{ji}(t). \quad (10)$$

Typically, Eq. (9) has also been expressed as a Fourier transform of a 2D exchange spectrum $S(\omega_1, \omega_2, t)$ by

$$F(t_1, t_2, t) = \int S(\omega_1, \omega_2, t) e^{-i\omega_1 t_1} e^{+i\omega_2 t_2} d\omega_1 d\omega_2. \quad (11)$$

Here, $S(\omega_1, \omega_2, t)$ is readily interpreted to be the joint probability of finding in the ensemble the frequency ω_1 at time

$t = 0$ and ω_2 at a later time t . 2D “exchange” spectroscopy is widely used^{15,17} not only to gain insight into the time scale, but also into the geometries of the corresponding molecular reorientation processes. In the case of powder samples, one often encounters well-defined elliptical patterns in 2D exchange NMR spectra from which discrete jump angles can readily be determined. 2D exchange experiments extend the working regime to ultraslow molecular jumps with rates below the effective coupling constant δ , the lower limit being the longitudinal relaxation rate T_1^{-1} .

3. 2D ^2H echo decay curves

Motivated by the formulation of the incoherent dynamic scattering function $S_{\text{inc}}(\mathbf{Q}, t)$ in quasielastic neutron scattering, there is an alternative¹⁸ for representing and using Eq. (10). Setting $t_1 = t_2 = \tau$ implies that we detect the amplitude of the stimulated echo only, though still obtain the full information on the molecular reorientation process. For $t \gg \tau$, in the case of ^2H NMR, one obtains

$$F(\tau, t) = \langle \exp[-i\tau\omega_Q(0)] \exp[i\tau\omega_Q(t)] \rangle, \quad (12)$$

which can be rewritten as¹⁰

$$F(\tau, t) = \int_0^\pi d\beta K_\beta(\tau) R(\beta, t). \quad (13)$$

Here

$$R(\beta, t) = \sum_{i,j=1}^N p_i P_{ji}(t) \delta(\beta - \beta_{ij}), \quad (14)$$

denotes the reorientation angle distribution at time t , with β_{ij} denoting the angle between orientations Ω_i and Ω_j . The integral kernel $K_\beta(\tau)$ contains information only on the physics of the spectroscopic method and is thus independent on the motional process under investigation. $K_\beta(\tau)$ acts as a filter, rendering the experiment more or less sensitive to different reorientation angles β , according to the adjustable parameter τ . Experimentally, it is worthwhile to measure the t -dependence of $F(\tau, t)$ for a set of τ -values. Here, we focus on the normalized final state correlation

$$F_\infty(\tau) = \frac{F(\tau, t \rightarrow \infty)}{F(\tau, t \rightarrow 0)}, \quad (15)$$

which may be viewed from the perspective of quasielastic neutron scattering as a generalized elastic incoherent structure factor (EISF). Finally, from inspection of Eq. (12) it can be seen that

$$\begin{aligned} F(\tau, t) &= \langle \cos[\tau\omega_Q(0)] \cos[\tau\omega_Q(t)] \rangle \\ &\quad + \langle \sin[\tau\omega_Q(0)] \sin[\tau\omega_Q(t)] \rangle \\ &= F^{\cos}(\tau, t) + F^{\sin}(\tau, t), \end{aligned} \quad (16)$$

where both parts, F^{\cos} and F^{\sin} , can be measured independently by proper rf-pulse phasing.

4. Static-field-gradient (SFG) ^1H NMR

Information on local reorientational dynamics obtained from methods (1)–(3) can be correlated with long-range dif-

TABLE I. Compositions and descriptions of the various benzene loaded NaY samples used in the experiments.

Sample #	Mean number of benzene molecules per supercage	Description
1	1.0	99.9% perdeuterated C ₆ D ₆
2	3.5	99.9% perdeuterated C ₆ D ₆
3	3.5	¹³ C ¹² C ₅ H ₆ 99% ¹³ C “single site” enriched C ₆ H ₆
4	5.1	99.9% perdeuterated C ₆ D ₆

fusion data acquired using magnetic-field gradients to spatially encode the ¹H signals. In a sufficiently strong magnetic-field gradient, the dominant dephasing mechanism arises from a spatially varying Larmor frequency

$$\omega[\mathbf{r}(t)] = \gamma B[\mathbf{r}(t)] = \gamma \mathbf{g} \cdot \mathbf{r}(t), \quad (17)$$

where γ is the gyromagnetic ratio, \mathbf{g} is the magnetic-field-gradient vector, and $\mathbf{r}(t)$ is the (possibly time dependent) spin position vector. With Eq. (17), the stimulated echo correlation function [Eq. (12)] can be reformulated after replacing ω_Q by $\omega[\mathbf{r}(t)]$. In the limit $t \gg \tau$, one can introduce the “generalized scattering vector” $\mathbf{Q} = \tau \gamma \mathbf{g}$ ¹⁷

$$F(\tau, t) = \langle e^{-i\mathbf{Q}\mathbf{r}(0)} e^{i\mathbf{Q}\mathbf{r}(t)} \rangle. \quad (18)$$

For Fickian diffusion (i.e., a Gaussian diffusion propagator), one obtains

$$F(\tau, t) \propto e^{-Q^2 D t}. \quad (19)$$

Note that the experiment not only yields a diffusion coefficient D , but also allows the spatial resolution to be selected by adjusting Q . Experimental deviations from Eq. (19) Q - t dependence due to finite crystallite size effects can be important in the NaY–benzene system and will be discussed below.

III. EXPERIMENTAL DETAILS

Commercial binder-free zeolite NaY (Si:Al=2.9; mean crystallite diameter of (0.5 ± 0.1) μm ; Degussa, Frankfurt, Germany) was placed in thin-walled NMR glass tubes (outer diameter 6 mm, length 20 mm). The samples were heated under vacuum ($\leq 10^{-3}$ Pa) at 400 °C for about 20 h applying a standard heating program.¹⁹ After cooling to ambient temperature, the zeolites were loaded with well defined amounts of the benzene isotopomers C₆D₆ (Merck, Darmstadt, Germany) or ¹³C¹²C₅H₆ (Isotec, Miamisburg, USA) and subsequently sealed under vacuum. Compositions and descriptions of the various samples are shown in Table I.

Solid-state NMR experiments were performed on three different instruments: (a) The ²H NMR data were acquired on a home-built spectrometer operating at a resonance frequency of $\omega_0/2\pi = 55$ MHz ($B_0 = 8.5$ T). High power rf-pulses ($\pi/2$ -pulse length ≈ 2.5 μs) were used to ensure broad band excitation. Receiver dead time effects in the 2D experiments were circumvented by using a five-pulse sequence with a 32-scan phase cycle.²⁰ Temperature control was achieved using a flow cryostat with a long term stability of about ± 0.2 K. (b) The ¹³C NMR spectra were acquired on a

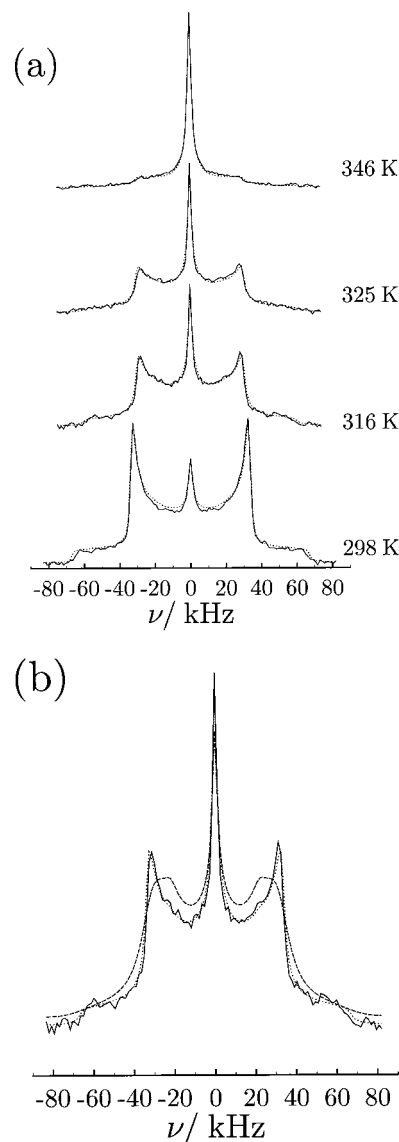


FIG. 1. (a) ²H echo NMR spectra of benzene adsorbed on NaY (5.1 molecules per supercage) at several temperatures. The pulse spacing was set to $\tau = 20$ μs . The experimental data are plotted as solid lines. Accompanying simulated spectra corresponding to the motional model (see text) are represented by the dotted plots. (b) ²H echo NMR spectrum as taken from (a) at 316 K. A fit with the tetrahedral jump model as defined by the rate matrix [Eq. (4)], i.e., with a single jump rate, is represented by the dashed plot, while the dotted line represents a fit including a distribution of correlation times [Eq. (18)]. Best fit parameters: $\tau_{\text{max}} = 3.9$ μs , $\sigma_{\tau} = 1.5$ decades.

commercial (Varian) spectrometer operating at 45.3 MHz ($B_0 = 4.2$ T) using ¹H–¹³C cross polarization enhancement and dipolar decoupling during the evolution and detection periods. (c) The ¹H diffusion data were acquired on a specialized home-built gradient NMR spectrometer. A key component of this spectrometer is an anti-Helmholtz-type superconducting magnet, which produces a magnetic field with a (static) gradient of up to 200 T/m.²¹

IV. RESULTS AND DISCUSSION

A. 1D echo spectra

Figure 1(a) shows one-dimensional solid-echo ²H NMR spectra of the benzene–NaY system (5.1 molecules per su-

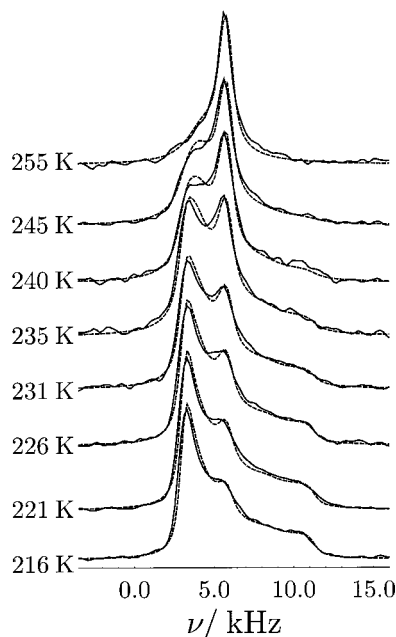


FIG. 2. ^{13}C echo NMR spectra of benzene adsorbed on NaY (3.5 molecules per supercage). The pulse spacing was $200\ \mu\text{s}$. Solid lines: Experimental data; dashed lines: simulated spectrum for a tetrahedral jump model with a distribution of correlation times, $\sigma_\tau \leq 1$ decade.

percentage) at several selected temperatures. At room temperature, the spectrum consists of a typical Pake pattern with a splitting of $\Delta\nu=69\ \text{kHz}$, along with a superimposed narrow peak in the center. With increasing temperature, the central line exhibits a constant width and grows in intensity at the expense of the broad spectrum, which also gradually changes its shape.

The low temperature NMR powder patterns are typical of benzene molecules performing rapid hexad axis reorientations (as discussed in Sec. II D above). The changes of the spectral line shape at higher temperatures are consistent with additional reorientations of the sixfold symmetry axis, as the adsorbed benzene molecules jump among tetrahedrally arranged cation and window sites. Figure 1(b) shows fits of the 316 K spectrum using such a tetrahedral jump model with a single correlation time (dotted line) and a log-normal distribution of correlation times [Eq. (5)] covering a width of $\sigma_\tau = 1.5$ decades (dashed line). There is a nearly perfect agreement between the model and the data across a wide temperature range [Fig. 1(a)] demonstrating the appropriateness of the jump model.

Figure 2 shows 1D ^{13}C echo NMR spectra obtained at several selected temperatures. The dashed lines again correspond to simulated spectra of benzene molecules in rapid hexad motion with additional tetrahedral jumps and a correlation time distribution as before, though with a narrower distribution of about 1.0 decade in width. Excellent agreement between simulation and experiment is observed for all loadings studied in this work, supporting the tetrahedral molecular jump model. The mean correlation times evaluated from these fits (Fig. 7) will be discussed below.

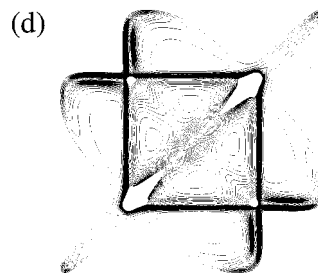
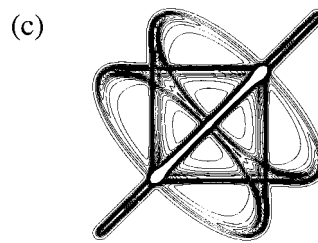
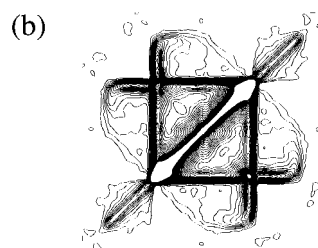
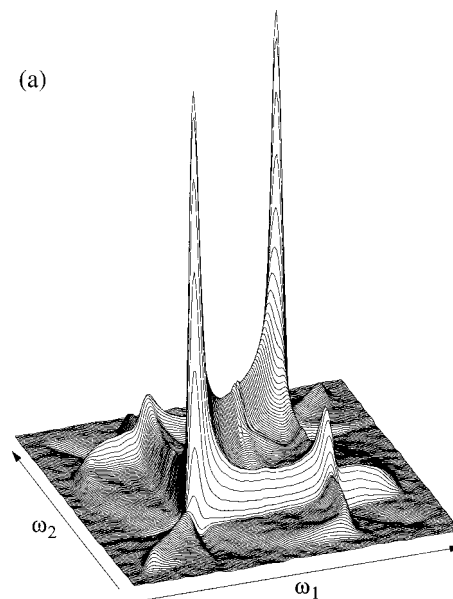


FIG. 3. (a) 2D exchange ^2H NMR spectrum of benzene adsorbed on NaY zeolite (5.1 molecules per supercage) for a mixing time of $t_{\text{mix}}=20\ \text{ms}$; (b) corresponding contour plot; (c) calculated contour plot for discrete well-defined tetrahedral jumps, and (d) for a Gaussian distribution of jump angles with a full width at half maximum $\Delta=6^\circ$ around an exact tetrahedral angle (109.5°).

B. 2D echo spectra

Figure 3(a) shows the 2D exchange ^2H NMR spectrum $S(\omega_1, \omega_2, t)$ [Eq. (11)] and Fig. 3(b) the corresponding contour plot obtained for benzene/NaY at 250 K containing 5.1

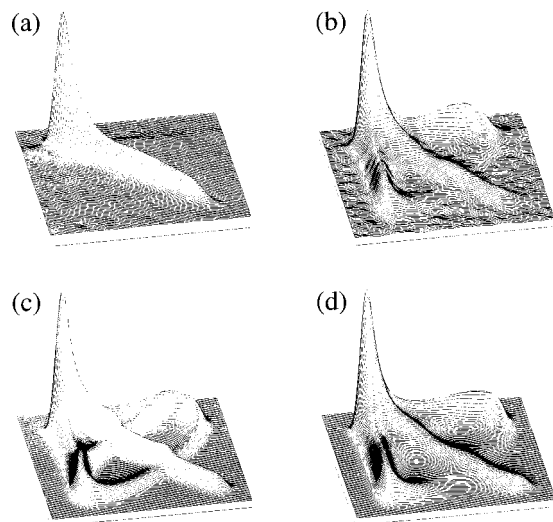


FIG. 4. 2D exchange ^{13}C NMR spectra of benzene adsorbed on NaY zeolite (3.5 molecules per supercage) at 188 K. Mixing times were (a) 1 ms and (b) 300 ms. Simulated final-state spectra are shown for the sharp tetrahedral jump model (c) and for a Gaussian distribution of jump angles with $\Delta=16^\circ$ (FWHM) around an exact tetrahedral angle (d).

adsorbed C_6D_6 molecules per supercage (sample #4). As reported previously,⁴ the spectrum can be reproduced using a tetrahedral jump model that leads to the elliptical patterns shown in Fig. 3(c). However, comparison of the simulated spectrum for the sharp tetrahedral jump motion with the experimental spectrum [Fig. 3(b)] shows some intensity differences, particularly alongside the diagonals near the center of the 2D plots. A significantly better match to the experimental spectrum is achieved by incorporating a distribution of reorientation angles into the simulation. A Gaussian distribution [full width at half maximum (FWHM) $\Delta=6^\circ$] of reorientation angles about the tetrahedral angle was employed. The width is necessary to account for the intensity near the diagonal [Fig. 3(d)]. Omitting this distribution [Fig. 3(c)] leads to sharper contours and poorer agreement with the experimental data.

Figure 4 shows experimental and simulated ^{13}C NMR spectra of sample #3 (3.5 $^{13}\text{C}^{12}\text{C}_5\text{H}_6$ “single site” enriched benzene molecules per NaY supercage). Again, the tetrahedral jump model with a jump angle distribution [$\Delta=16^\circ$, Fig. 4(d)] produces a better match to the experimental data than the exact tetrahedral-jump model [Fig. 4(c)]. These results provide consistent evidence for a distribution of molecular jump angles in the fully (5.1 molecules per supercage) and intermediate (3.5 molecules per supercage) loaded benzene–NaY zeolite samples.

C. 2D echo decays

2D ^2H echo time domain measurements $F(\tau, t)$ [Eqs. (12), (13), (16)] provide a more quantitative basis for analyzing the molecular jump angle distributions. At the highest loading (5.1 benzene molecules per NaY supercage, sample #4), a distribution of jump angles has previously been established with ($\Delta=5^\circ\text{--}7^\circ$ FWHM) about an exact tetrahedral angle.⁴ Further, there is a distribution of correlation times which can be described by a Kohlrausch exponent of β_K

≈ 0.7 or, equivalently, by a width parameter of $\sigma_\tau \approx 1$ decade. From the τ -dependence of the mean correlation time $\langle \tau_c \rangle$, it has been proposed that small angle relaxations of the local environment of a benzene molecule occur just after a tetrahedral jump event.

The jump angle and the correlation time distributions both likely arise due to the dynamic disorder present in the benzene subsystem. This is substantiated by 2D echo decay data on NaY zeolite samples with different concentrations of adsorbed benzene. Both contributions $F^{\cos}(\tau, t)$ and $F^{\sin}(\tau, t)$ to $F(\tau, t)$ [Eq. (16)] have been measured on sample #2 (3.5 C_6D_6 per supercage) and $F^{\cos}(\tau, t)$ on sample #1 (1.0 C_6D_6 per supercage), with the geometry parameter τ varied between 1 and 100 μs . As previously found,⁴ the time-dependent ^2H decay curves reveal two regimes, one due to molecular motion and a second arising from spin-lattice relaxation. Parametrization with

$$F^{\cos/\sin}(\tau, t) = \left\{ A(\tau) \exp \left[- \left(\frac{t}{\tau_K(\tau)} \right)^{\beta_K(\tau)} \right] + B(\tau) \right\} e^{-t/T_1}, \quad (20)$$

yields final-state correlations

$$F_\infty^{\cos/\sin}(\tau) = \frac{B(\tau)}{A(\tau) + B(\tau)}, \quad (21)$$

which are shown in Fig. 5. The figure also contains calculated final-state curves modelled with perfect and distorted tetrahedral jumps. Distorted tetrahedral reorientations are modelled by a Gaussian broadening of the sharp contributions in the tetrahedral jump angle distribution. The plots indicate that orientational disorder characterized by a Gaussian width parameter of $\Delta=16^\circ$ fits both samples best. At lower benzene loadings, the reorientation angle distributions are thus broader, indicating that the tetrahedral symmetry of the benzene adsorption sites is more distorted at lower coverages. The stretching parameters $\beta_K(\tau)$ for samples #1 (1.0 C_6D_6 per supercage), #2 (3.5 C_6D_6 per supercage), and #4 (5.1 C_6D_6 per supercage) have been shown⁴ to be independent of τ and equal to ≈ 0.7 . This corresponds to a Gaussian correlation time distribution width of about 1 decade, which is consistent with the 1D ^2H echo analyses discussed above.

Turning to the τ -dependence of the “Kohlrausch” time constant τ_K (Fig. 6), a significantly different behavior is observed for sample #1 (1.0 C_6D_6 per supercage), compared to samples with higher loadings, such as sample #2 (3.5 C_6D_6 per supercage), and #4 (5.1 C_6D_6 per supercage). This difference at low adsorbate concentrations is one of key results of this work and will be discussed in detail below. As has been pointed out in Ref. 18, the integral kernel $K_\beta(\tau)$ [see Eq. (13)] renders the experiment, at small values of τ , highly sensitive to large angle reorientations only and, at large τ -values, sensitive to small angle reorientations as well. A quantitative fit to the experimental results $\tau_K(\tau)$ for the highly loaded sample #4 (5.1 C_6D_6 per supercage) with a model assuming two time constants, τ_1 for well-defined tetrahedral jumps, and τ_2 for concomitant small angle jumps, was performed and discussed in Ref. 4. The best fit was obtained for $\tau_1/\tau_2 \approx 2$, which was interpreted to arise from

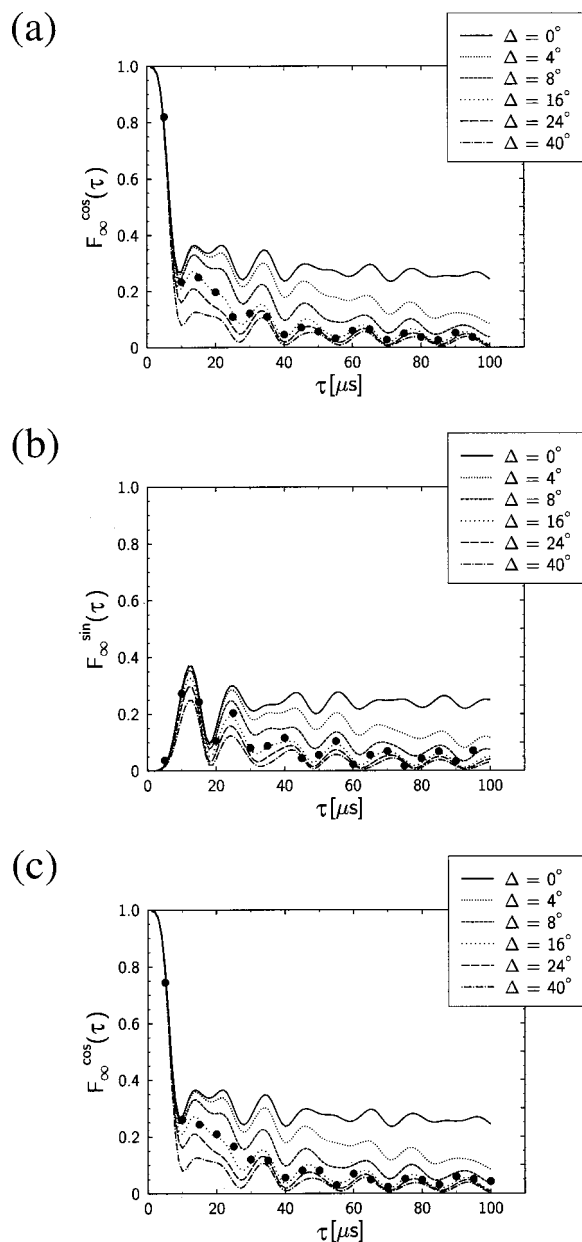


FIG. 5. Final-state values of the 2D ^2H echo decay curves: (a) $F_{\infty}^{\cos}(\tau)$ and (b) $F_{\infty}^{\sin}(\tau)$ of sample #2 (3.5 benzene molecules per NaY supercage) and (c) $F_{\infty}^{\cos}(\tau)$ of sample #1 (1.0 molecules per supercage). The experimental data, as obtained from the parametrization of Eqs. (20) and (21), are indicated by the symbol (\bullet). The curves are the result of model calculations for different values of Δ , which parameterize the width of the jump angle distributions.

small angle adjustments by approximately two adsorbed molecules in response to a tetrahedral jump made by another molecule. This is further supported by the observation that, apart from a temperature-dependent scaling factor, $\tau_K(\tau)$ is the same at all temperatures. It is not surprising that $\tau_K(\tau)$ is essentially the same for both sample #2 (3.5 C_6D_6 per supercage) and sample #4 (5.1 C_6D_6 per supercage), but different for sample #1 (1.0 C_6D_6 per supercage). Sample #1 has on average a single benzene molecule in each supercage, thus lacking other neighboring adsorbed molecules in the same cage to relax. Experimentally, this is reflected by the τ -independence of τ_K .

By examining the temperature-dependence of the mo-

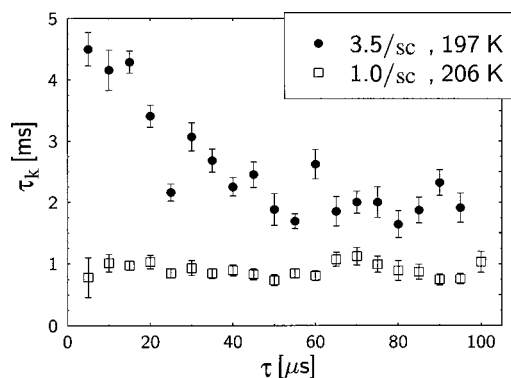


FIG. 6. “Kohlrausch” time constants $\tau_K(\tau)$ measured for benzene adsorbed on NaY zeolite at average bulk loadings of 1 (sample #1) and 3.5 (sample #2) molecules per supercage, obtained by parametrization of the measured stimulated echo decay curves with Eq. (20).

tional correlation times $\langle\tau_c\rangle$, Arrhenius-type activation energies can be determined for the slow tetrahedral molecular jump processes. As far as the 2D echoes are concerned, fixed values have been assigned to the geometry parameter τ (^2H -NMR: $\tau=10\ \mu\text{s}$; ^{13}C -NMR: $\tau=160\ \mu\text{s}$), which are small enough to ensure that tetrahedral jumps dominate the decays. Figure 7, as discussed above, summarizes the correlation time data $\langle\tau_c\rangle$ from the 1D NMR spectra and 2D echo decays, discussed in Secs. IV A and IV B, respectively.

The figure clearly demonstrates the complementary combination of the two methods, which enlarges the dynamic range of the measurements up to almost five decades. Over the temperature range 170–350 K, all samples display Arrhenius behaviors, indicating that thermally activated molecular dynamic processes dominate in this temperature regime. The highest and lowest loaded samples have been fit to purely Arrhenius functions, $\langle\tau_c\rangle^{-1} = \tau_{\infty}^{-1} \exp[-E_a/RT]$, where E_a is the apparent activation energy and τ_{∞}^{-1} is the corresponding pre-exponential factor. In the case of the intermediately loaded sample, 3.5 molecules per supercage, lower temperatures were probed, revealing that $\langle\tau_c\rangle(T)$ levels off at reduced temperatures (below 160 K). This is attrib-

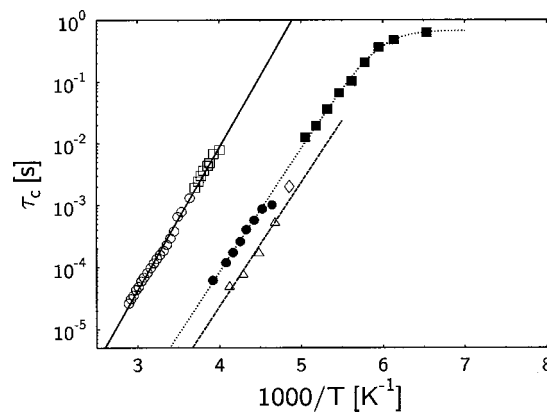


FIG. 7. Mean motional correlation times of benzene molecules undergoing tetrahedral jumps as a function of inverse temperature at different benzene loadings. 1.0 molecules per supercage: \triangle — ^2H 1D echo, \diamond — ^2H 2D echo decay; 3.5 molecules per supercage: \bullet — ^{13}C 1D echo, \blacksquare — ^{13}C 2D echo decay; 5.1 molecules per supercage: \circ — ^2H 1D echo, \square — ^2H 2D echo decay. The straight lines are Arrhenius fits to the data.

TABLE II. Experimental activation energies and preexponential factors for tetrahedral jump processes undergone by benzene molecules adsorbed on NaY zeolite at different loadings.

5.1 molecules per supercage	$E_a = 44.5 \pm 0.5$ kJ/mol $\tau_\infty = (4.6 \pm 0.8) \times 10^{-12}$ s
3.5 molecules per supercage	$E_a = 38.4 \pm 0.3$ kJ/mol $\tau_\infty = (0.78 \pm 0.13) \times 10^{-12}$ s $\tau_{SD} = 0.68 \pm 0.04$ s
1.0 molecules per supercage	$E_a = 38.8 \pm 4.2$ kJ/mol $\tau_\infty = (0.22 \pm 0.10) \times 10^{-12}$ s

uted to temperature-independent spin diffusion, which has previously been examined in detail for the benzene–Ca-LSX zeolite system.⁵ This is further supported by the observation that in this regime β_K tends to increase toward a value of unity. [Spin diffusion (SD), which is due to pair-wise dipolar interactions, is relatively insensitive to disorder.] For the intermediately loaded sample, therefore, a temperature-independent spin diffusion rate τ_{SD}^{-1} has been added, $\langle \tau_c \rangle^{-1} = \tau_\infty^{-1} \exp[-E_a/RT] + \tau_{SD}^{-1}$, which yields the corresponding best fit curve. Table II summarizes the fit parameters and results which will be discussed in more detail below.

D. Intracrystallite diffusion

Determining diffusivities of guest molecules in zeolites with small crystallite dimensions ($< 1 \mu\text{m}$) is usually difficult. This is because the magnetic-field gradients used in conventional pulsed-field-gradient (PFG) NMR methods are often not strong enough to identify intracrystallite diffusion. Under such circumstances, PFG measurements may include contributions from intra- and intercrystallite diffusion. As a consequence, it is necessary to analyze the experimental data²² in terms of diffusion models, which include boundary conditions at the crystallite surface.^{23–25} However, such results depend inherently on the adoption of a suitable model and thus issues of uniqueness remain.

An alternate approach is to use very high static magnetic-field gradients to allow smaller ($< 1 \mu\text{m}$) molecular displacements to be probed, so that only the intracrystallite contribution to diffusion is relevant.¹⁸ For sufficiently large Q -values, the difficult-to-characterize boundary effects become unimportant, such that Eq. (19) holds in an asymptotic limit. In this case, the diffusion path lengths become short enough to measure intracrystallite translational diffusion. Here, this limit is approached, though not completely so, as established by static-field-gradient NMR measurements performed over a wide range of Q -values.

For intracrystallite Fickian diffusion and $t \gg \tau$, $F(\tau, t)$ would be given by Eq. (19). Often, however, the condition $t \gg \tau$ cannot be fulfilled experimentally. In such cases, one can overcome this limitation by introducing an effective diffusion time, $t + 2\tau/3$ that leads to²⁶

$$F(\tau, t) = \exp[-\gamma^2 g^2 \tau^2 D(t + 2\tau/3)]. \quad (22)$$

Accounting for T_1 - and T_2 -relaxation, the stimulated echo amplitude M is related to $F(\tau, t)$ via

$$M(\tau, t) \propto F(\tau, t) e^{-2\tau/T_2} e^{-t/T_1}. \quad (23)$$

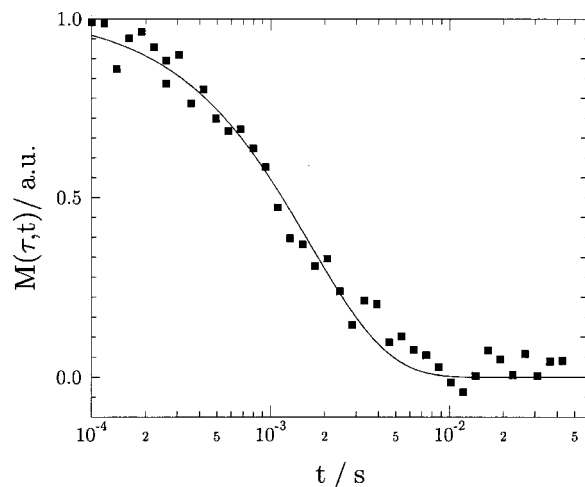


FIG. 8. Stimulated echo decay of the ^1H NMR signal measured at 390 K for benzene–NaY (3.5 molecules per supercage, sample #3) at a resonance frequency of 75 MHz in a static magnetic field gradient of $g = 175$ T/m (evolution time $\tau = 400 \mu\text{s}$, corresponding to $Q = \tau \gamma g = 18.7 \mu\text{m}^{-1}$). The data were fitted using Eq. (23).

Because of the notoriously low sensitivity of static-field-gradient NMR,²⁷ diffusion measurements have been limited to the protonated sample #3 (3.5 $^{13}\text{C}^{12}\text{C}_5\text{H}_6$ benzene molecules/supercage). Figure 8 shows a typical benzene ^1H NMR stimulated echo decay curve measured in a magnetic-field gradient of 175 T/m and its accompanying fit obtained using Eqs. (22) and (23). The T_1 -parameter was measured independently using a saturation recovery pulse sequence in the gradient spectrometer. In this way, the Q -dependence of the apparent diffusion coefficient at two different temperatures was determined, as shown in Fig. 9. In these experiments, the Q values have been adjusted by either varying the evolution time, τ , within the range permitted by T_2 -relaxation [e.g., $T_2 = 920(20) \mu\text{s}$ at 450 K] and/or by changing the gradient strength, g . The strong decrease of the apparent diffusion coefficient with increasing Q reflects the influence of the crystallite grain boundaries. From Fig. 9 alone it is not obvious how to deduce the intracrystallite

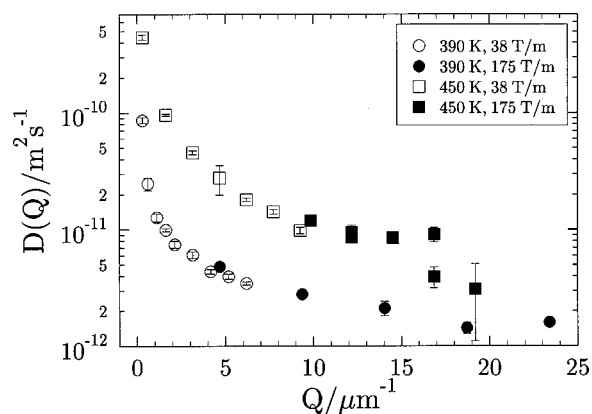


FIG. 9. Apparent benzene diffusion coefficients $D(Q)$ measured for benzene–NaY, 3.5 benzene molecules per supercage (sample #3) at 390 and 450 K and using different static field gradient strengths of 38 or 175 T/m. The diffusivities have been extracted from fits of the data using Eqs. (22) and (23).

diffusion coefficient quantitatively. The $D(Q)$ data level off into a constant plateau value at around $Q^* \cong 10 \mu\text{m}^{-1}$ which corresponds to a crystallite size of (very roughly) $2\pi/Q^* \cong 0.6 \mu\text{m}$, a value which is in reasonable consistency with that known from scanning electron microscopy. In this sense, the data at the highest Q -values represent an estimate of the upper bound for the intracrystallite diffusion coefficient $D(T)$.

E. Discussion: Diffusion and local dynamics

For establishing a unified picture that is consistent with both the microscopic and mesoscopic data, the diffusion coefficient D can be traced back to elementary jump processes, which yield^{28,29}

$$D = \frac{1}{6} W a^2, \quad (24)$$

where W is the mean jump rate of a benzene molecule from an adsorption site into the center of a neighboring supercage and a is the distance between neighboring supercages. From structural data, a is known to be $\approx 1.1 \text{ nm}$.³⁰

Assuming that W is proportional to the jump rate observed in local spectroscopy

$$W = (1/\alpha) w, \quad (25)$$

and inserting $w = 1/(4\tau_c)$ [Eq. (4)], we can relate W and, therefore, D to the experimental correlation times τ_c according to

$$\tau_c^{-1} = \alpha 24 D / a^2. \quad (26)$$

The proportionality factor α depends on the jump mechanism. If the SII Na^+ cations are the energetically favored adsorption sites and jumps from a window to SII sites are governed by a low activation energy,^{31,32} then $w = w_{\text{SII} \rightarrow w}$ leads to a dominant rate relevant for diffusion with $W = 2w$. (The factor of 2 accounts for the fact that four window sites are accessible and the probability to jump from a window site into a neighboring supercage is 1/2.) In other words, $\alpha = 1/2$. Note that other jump mechanisms may lead to slightly different values of α .

Under the above assumptions Eq. (26) allows the measured diffusion coefficients (as extrapolated from Fig. 9) to be converted into elementary jump correlation times and compared to those obtained from 1D and 2D NMR spectroscopy, Fig. 10. The solid line in Fig. 10, which represents the Arrhenius fit to the local jump rates (using the parameters of Table II), is extrapolated into the temperature range of the diffusion data. Despite the uncertainty in the diffusion data, the rates obtained from local spectroscopy measurements look qualitatively consistent with the assumptions leading to Eqs. (25) and (26). However, the fact that the extrapolated local jump rates roughly agree with those obtained from diffusion data should not be overinterpreted. Qualitatively, one may conclude that the jumps observed in local spectroscopy might be the elementary processes responsible for long-range diffusion and that the low temperature activation energy persists up to the diffusion-dominated regime. However, firm conclusions concerning the associated activation barriers cannot meaningfully be made, based on the two diffusion data points available.

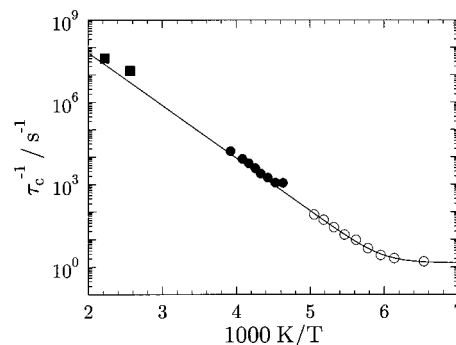


FIG. 10. Elementary jump rates of benzene molecules adsorbed on NaY zeolite, 3.5 molecules per NaY supercage, (sample #3) obtained from static-field-gradient NMR (■), ^{13}C 1D echo line shapes (●) and ^{13}C 2D echo decay curves (○). The full curve results from a fit to the low-temperature data with parameters taken from Table II.

V. CONCLUSIONS

Application of complementary 1D and 2D solid-state ^2H and ^{13}C NMR spectroscopy techniques leads to a consistent picture of the dynamics and transport properties of benzene molecules adsorbed on NaY zeolite. The exchange of benzene molecules among the tetrahedrally arranged adsorption sites results in reorientations of the molecular symmetry axes, which are detected in the NMR experiment. The reorientation angles differ from an exact tetrahedral jump process, due to site occupancy disorder in the guest system. This kind of orientational disorder is less pronounced at higher loadings. A detailed analysis of the data indicates that small-angle reorientations accompany the tetrahedral jumps. These small angle jumps stem from a rapid adjustment of the orientations of neighboring molecules adsorbed in close proximities to the molecule undergoing a tetrahedral jump event. At a sufficiently low bulk loading (e.g., 1 molecule per supercage), no accompanying small-angle molecular reorientations are observed, consistent with the relatively low probability of finding molecules near one another at low coverage. The 2D echo correlation functions decay nonexponentially. This is interpreted in terms of a distribution of tetrahedral jump rates, which is observed in 1D NMR echo line shapes as well.

Using strong static-magnetic-field gradients, we have been able to estimate limits for intracrystallite benzene self diffusion. Comparisons of the diffusion coefficient(s) with the local jump rate suggests a common origin of both dynamic processes. Finally by using static-field gradients of almost 200 T/m, new experimental limits have been reached in the effort to examine macroscopic intracrystallite transport of guest hydrocarbon species. Yet, for the small (submicron) NaY crystallites used in the present study, the diffusion results remain influenced by crystallite boundary effects and intercrystallite contributions. While little more can be done to extend the gradient NMR approach using current technology, there may be several ways to approach this challenge. These include using larger crystallite sizes ($>1 \mu\text{m}$), in combination with strongly adsorbing guest molecules that diffuse slowly, and lower temperatures. Another possibility would be to use an approach that would enable larger Q values to be

reached, such as combining NMR and quasielastic neutron scattering methods. An alternative approach to the problem might be based on an understanding of crystallite surface effects themselves. A more detailed understanding of the molecular dynamic and macroscopic diffusional processes of guest species in zeolites will require continued development of improved experimental and theoretical capabilities.³³

ACKNOWLEDGMENTS

The work has been carried out within the framework of the Graduiertenkolleg "Festkörperspektroskopie" and "Struktur-Dynamik Beziehungen in mikrostrukturierten Systemen" at the Universität Dortmund, sponsored by the Deutsche Forschungsgemeinschaft (DFG). Support from NATO Collaborative Research Grant No. 973083 and the USARO under grant DAAH04-96-1-0443 is gratefully acknowledged by two of us (B.F.C. and D.E.F.).

¹G. T. Kokotailo and C. A. Fyfe, *J. Phys. Chem. Solids* **50**, 441 (1989).

²A. Dyer, *An Introduction to Zeolite Molecular Sieves* (Wiley, New York, 1988).

³N. Y. Chen, T. F. Degnan, and C. M. Smith, *Molecular Transport and Reaction in Zeolites* (VCH, New York, 1994).

⁴O. Isfort, B. Boddenberg, F. Fujara, and R. Grosse, *Chem. Phys. Lett.* **288**, 71 (1998).

⁵D. J. Schaefer, D. E. Favre, M. Wilhelm, S. J. Weigel, and B. F. Chmelka, *J. Am. Chem. Soc.* **119**, 9252 (1997).

⁶D. E. Favre, D. J. Schaefer, S. A. Auerbach, and B. F. Chmelka, *Phys. Rev. Lett.* **81**, 5852 (1998).

⁷A. Gédéon, D. E. Favre, J. MacNeil, D. Reichert, and B. F. Chmelka, *J. Phys. Chem. A* **103**, 6691 (1999).

⁸H. Sillescu, *J. Chem. Phys.* **104**, 4877 (1996).

⁹N. G. van Kampen, *Stochastic Processes in Physics and Chemistry* (Elsevier Science, Amsterdam, 1981).

¹⁰F. Fujara, S. Wefing, and W. F. Kuhs, *J. Chem. Phys.* **88**, 6801 (1988).

¹¹B. Geil, F. Fujara, and H. Sillescu, *J. Magn. Reson.* **130**, 18 (1998).

¹²H. Lechert and K. P. Wittern, *Ber. Bunsenges. Phys. Chem.* **83**, 596 (1979).

¹³V. Voss and B. Boddenberg, *Surf. Sci.* **298**, 241 (1993).

¹⁴M. S. Greenfield, A. D. Ronemus, R. L. Vold, and R. R. Vold, *J. Magn. Reson.* (1969-1992) **72**, 89 (1987).

¹⁵D. W. Alderman, M. S. Solum, and D. M. Grant, *J. Chem. Phys.* **84**, 3717 (1986).

¹⁶K. Schmidt-Rohr and H. W. Spiess, *Multidimensional Solid-State NMR and Polymers* (Academic, London, 1984).

¹⁷R. Kimmich, *NMR Tomography, Diffusometry, Relaxometry* (Springer, Berlin, 1997).

¹⁸G. Fleischer and F. Fujara, in *NMR, Principles and Progress*, edited by P. Diehl, E. Fluck, H. Günther, R. Kosfeld, and J. Seelig (Springer, Berlin, 1994), Vol. 30.

¹⁹B. Boddenberg and A. Seidel, *J. Chem. Soc., Faraday Trans.* **90**, 1345 (1994).

²⁰D. Schäfer, J. Leisen, and H. W. Spiess, *J. Magn. Reson.* **115**, 50 (1995).

²¹I. Chang, F. Fujara, B. Geil, G. Hinze, H. Sillescu, and A. Tölle, *J. Non-Cryst. Solids* **172**, 674 (1994).

²²N. K. Bär, S. Ernst, J. Kärger, H. B. Schwarz, and J. Weitkamp, *Microporous Mater.* **6**, 355 (1996).

²³P. P. Mitra and P. N. Sen, *Phys. Rev. B* **45**, 143 (1992).

²⁴P. P. Mitra, P. N. Sen, and L. M. Schwartz, *Phys. Rev. B* **47**, 8565 (1993).

²⁵P. T. Callaghan, *J. Magn. Reson.* **113**, 53 (1995).

²⁶E. O. Stejskal and J. E. Tanner, *J. Chem. Phys.* **42**, 288 (1965).

²⁷B. Geil, *Concepts Magn. Reson.* **10**, 299 (1998).

²⁸S. M. Auerbach and H. I. Metiu, *J. Chem. Phys.* **105**, 3753 (1996).

²⁹S. M. Auerbach, *J. Chem. Phys.* **106**, 7810 (1997).

³⁰B. Boddenberg and R. Burmeister, *Zeolites* **8**, 488 (1988).

³¹S. M. Auerbach, N. J. Henson, A. K. Cheetham, and H. I. Metiu, *J. Phys. Chem.* **99**, 10600 (1995).

³²S. M. Auerbach and H. I. Metiu, *J. Chem. Phys.* **106**, 2893 (1997).

³³J. Kärger and P. Volkmer, *J. Chem. Soc., Faraday Trans. 1* **76**, 1562 (1980).